# Using Raman Spectroscopy to Elucidate the Aggregation State of Single-Walled Carbon Nanotubes

**Daniel A. Heller,[†] Paul W. Barone,[‡] John P. Swanson,[‡] Rebecca M. Mayrhofer,[‡] and Michael S. Strano*[,‡]**

*Department of Chemistry and Department of Chemical and Biomolecular Engineering, University of Illinois at Urbana−Champaign, Urbana, Illinois 61801*

*Received: December 3, 2003; In Final Form: March 29, 2004*

Raman spectroscopy can be used to probe the aggregation state of single-walled carbon nanotubes in solution or as solids with a range of varying morphologies. Carbon nanotubes experience an orthogonal electronic dispersion when in electrical contact that broadens (from 40 meV to roughly 80 meV) and shifts the interband transition to lower energy (by 60 meV). We show that the magnitude of this shift is dependent on the extent of bundle organization and the inter-nanotube contact area. In the Raman spectrum, aggregation shifts the effective excitation profile and causes peaks to increase or decrease, depending on where the transition lies, relative to the excitation wavelength. The results are modeled using a simplified $\delta$-function representation of nanotube electronic structure. The findings are particularly relevant for evaluating nanotube separation processes, where relative peak changes in the Raman spectrum can be confused for selective enrichment.

## Introduction

Single-walled carbon nanotubes (SWNT) are an important class of materials for novel electronic,[1] optical,[2,3] and structural composite[4−6] technologies. For the former two applications in particular, carbon nanotubes need to be sorted and separated by their different electronic structures. Variation in electronic structure follows from the quantization of the electronic wave function as the graphene plane is conceptually rolled into a cylinder forming a nanotube.[7,8] The vector in units of the hexagonal elements connecting the path tracing the nanotube circumference defines the chirality in terms of two integers: $n$ and $m$. This chirality vector ($n$,$m$) determines the electronic properties: when $|n - m| = 3q$ where $q$ is an integer, the nanotube is metallic or semi-metallic while remaining species are semiconducting with a diameter and chirality dependent band-gap. All known synthetic methods for producing carbon nanotubes yield a range of these electronic types,[8−10] typically as a distribution function about a mean tube diameter.[11] Separating and sorting nanotubes according to their electronic structure remains a central hurdle to their widespread application. Only recently have researchers begun to seriously address this problem.[12−16]

To this end, the peaks in the low-wavenumber region of the SWNT Raman spectrum are frequently used as a measure of the relative populations of particular carbon nanotubes.[8,17,18] The known diameter dependence of these radial breathing modes (RBMs) allows for an almost direct identification of particular ($n$,$m$) species in the sample that are resonant at the particular excitation wavelength.[2,19] Several recent investigations have compared relative changes to the intensities of these modes, in the effort to benchmark the separation processes.[13−15] In addition, the tangential mode region of 1500−1600 cm$^{-1}$ in the Raman spectrum can identify the presence of metallic and semiconducting nanotubes, because the former results in a Breit−Wigner−Fano (BWF) line shape. Here, the discrete tangential phonon couples to the continuum of electronic states at the Fermi level.[17,18,20]

Despite the widespread use of these features in benchmarking separation processes, several complications arise that may lead to inaccurate conclusions regarding separation. Moreover, understanding the relationship between aggregation and spectroscopy would benefit efforts to functionalize nanotubes,[13] make well-dispersed nanotube composites,[21] or use Raman spectroscopy to monitor other nanotube processing techniques. The strong resonant enhancement of the SWNT Raman spectrum is well-documented.[8,17−19] Samples in different physical[3] or chemical[22] environments can exhibit variations in the relative intensities of various Raman modes. Previous investigations have begun to explore the effects of aggregation[23] and chemical environment[22,24,25] on these spectra. In this work, we correlate systematic changes in the Raman spectrum to variations in sample morphology characterized by microscopy.

## Experimental Section

Nanotubes synthesized by the HiPco process were suspended in a 1% sodium dodecyl sulfate (SDS) solution, using a previously described procedure.[3,22] Acetone was added to flocculate and remove nanotubes from this solution. The flocculant mass was then washed with methanol to remove excess surfactant. Nanotubes were precipitated from the SDS solution by heating and evaporating the liquid on a microscope slide. Dried nanotubes were washed in methanol to remove SDS. Scanning electron microscopy (SEM) was performed by depositing nanotubes on a silicon wafer and imaging with a Hitachi S4700 SEM system. Cryo-transmission electron microscopy (cryo-TEM) measurements were conducted as described by Moore et al.[26] Raman spectra were obtained at 785 nm, with a Kaiser model RamanRXN1 analyzer, and at 514.5 nm, using a

* Author to whom correspondence should be addressed. Fax: 217-333-5052. E-mail address: strano@uiuc.edu.
[†] Department of Chemistry.
[‡] Department of Chemical and Biomolecular Engineering.

10.1021/jp037690o CCC: $27.50 © 2004 American Chemical Society
Published on Web 04/29/2004

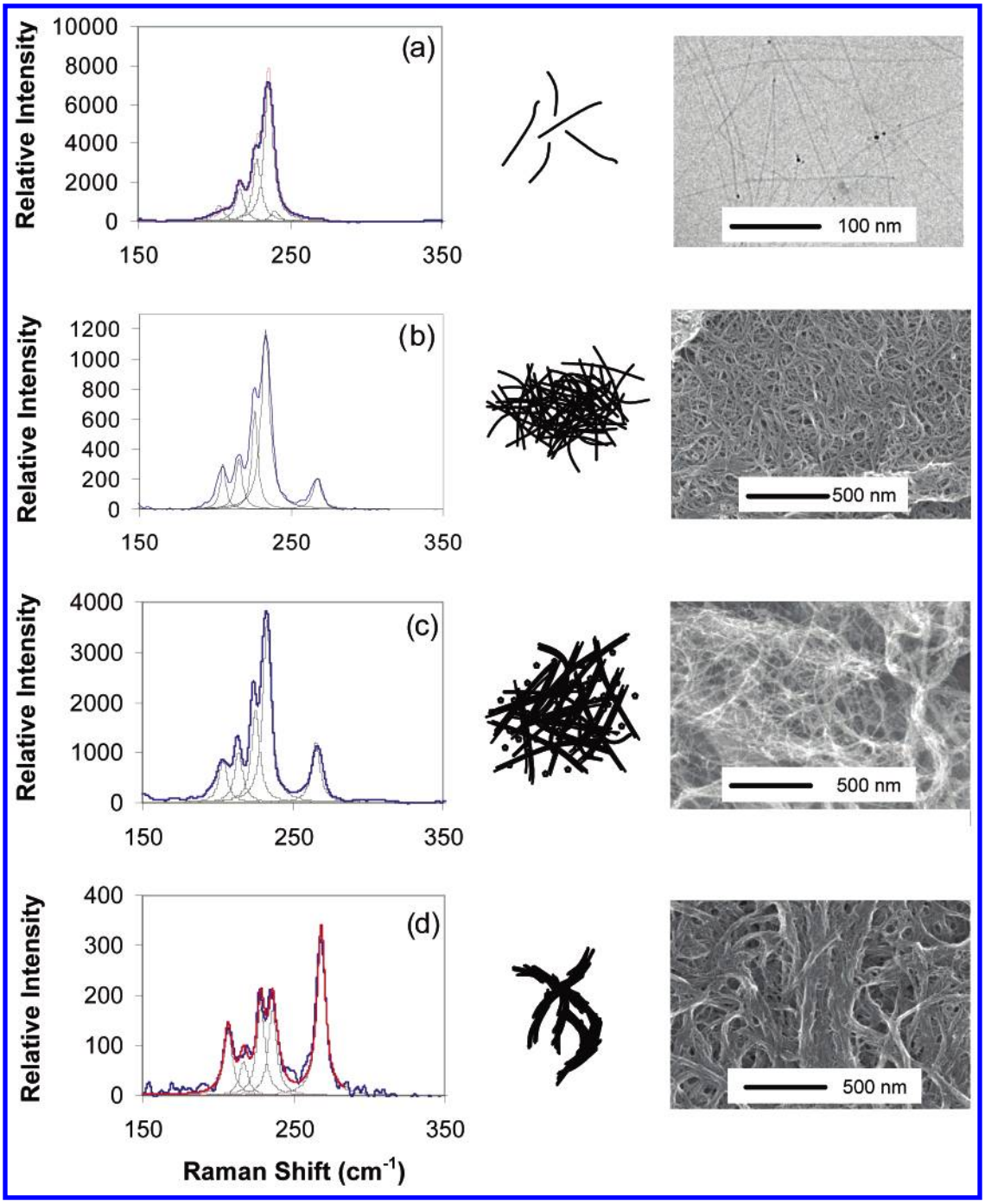


**Figure 1.** Raman spectra taken at 785 nm with scanning electron microscopy (SEM) micrographs and represented aggregation states for four samples prepared with different morphologies. Radial breathing mode (RBM) regions are shown for (a) a sample dispersed in aqueous solution using 1 wt % sodium dodecyl sulfate (SDS) at pH 10, (b) HiPco nanotubes flocculated from solution with acetone and washed in methanol, (c) HiPco single-walled carbon nanotube (SWNT) used as received, and (d) nanotubes precipitated on a glass slide from SDS solution and washed to remove surfactant.

Spectra Physics model 2000 $Ar^+$ laser with a SPEX model 1877 Triplemate triple-grating monochromator and a Princeton Instruments model SPEC-10 400B digital charge-coupled device (CCD) camera.

## Results

In Figure 1, four different HiPco SWNT samples are compared at an excitation of 785 nm, using the RBM region. In Figure 1a, we show the material dispersed in 1% SDS/$H_2O$ at pH 10. This material was flocculated from solution to produce Figure 1b. This is compared to material used as received with 50% iron catalyst (by weight) and unprocessed after reactor synthesis (Figure 1c). Finally, if the material in Figure 1a is precipitated from solution, the spectrum in Figure 1d is obtained. Graphics beside the spectra depict the believed aggregation state of the material, which generally increases from Figure 1a to Figure 1d. SEM and cryo-TEM micrographs of the samples show evidence of this aggregation. A cryo-TEM image of nanotubes[26] suspended in SDS (Figure 1a) shows individual nanotubes dispersed in solution, displaying minimal intertube contact. The flocculated nanotubes (Figure 1b) associate into mats of loosely aggregated nanotubes. Raw HiPco SWNT that have not been previously dispersed exhibit wound bundles, mats, and various other morphologies (Figure 1c). The nanotubes

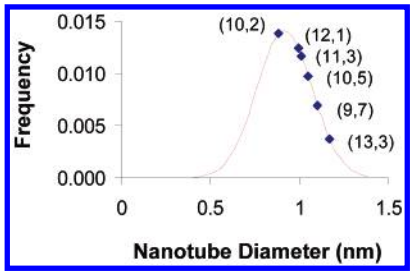


**Figure 2.** Estimated concentration distribution of SWNT diameters of the six HiPco nanotubes present in the 785-nm Raman spectrum.

precipitated from SDS (Figure 1d) form tightly roped bundles. The spectral comparison reveals substantial diminution of the prominent mode at 234 $cm^{-1}$ and an increase in one at 267 $cm^{-1}$. Previous work shows that the latter increases absolutely, not merely relative to other modes.[23] The significant variability in relative intensities in this region is echoed at other Raman excitation wavelengths and raises concerns about using this region exclusively to make statements about sample composition.

As nanotubes aggregate into parallel, aligned contact, their $k_z$-band structure is altered and they develop an orthogonal electronic dispersion to their otherwise one-dimensional (1-D) axial dispersion along the tube length. Reich et al. have accurately modeled this process using ab initio calculations.[27] In practice, the absorption spectrum of nanotube bundles is red-shifted and broadened, compared with pristine nanotubes.[3,23] These changes to the absorption line shape affect the Raman spectrum in several ways. Most notably, a species may be selectively brought into resonance, resulting in an increase in the overall scattering intensity. The converse is also possible. As an aside, note that, within the resolution of the spectrometer used in this work (4 $cm^{-1}$), there is no shifting of the RBM peak center with aggregation, as anticipated by experimental high-pressure studies and molecular dynamics simulations.[28]

## Discussion

Some insight is gained upon closer examination of the data in Figure 1. We have modeled this process at 785 nm in detail, using the spectral assignment of the nanotubes in Figure 1. We assume a simple, Gaussian distribution, with regard to the nanotube diameter $d_t$ ($\sigma = 0.2$ nm, $d_{mean} = 0.93$ nm) for the relative intensities of the highly dispersed material. Figure 2 shows the location of six ($n$,$m$) nanotubes within the assumed distribution. Describing each feature as a Lorentzian line shape in the Raman spectrum with a shift given by $223.5/d_t + 25.5$, the Raman intensity ($I(E_{Laser})$) of each feature is described, assuming that the corresponding interband transition can be

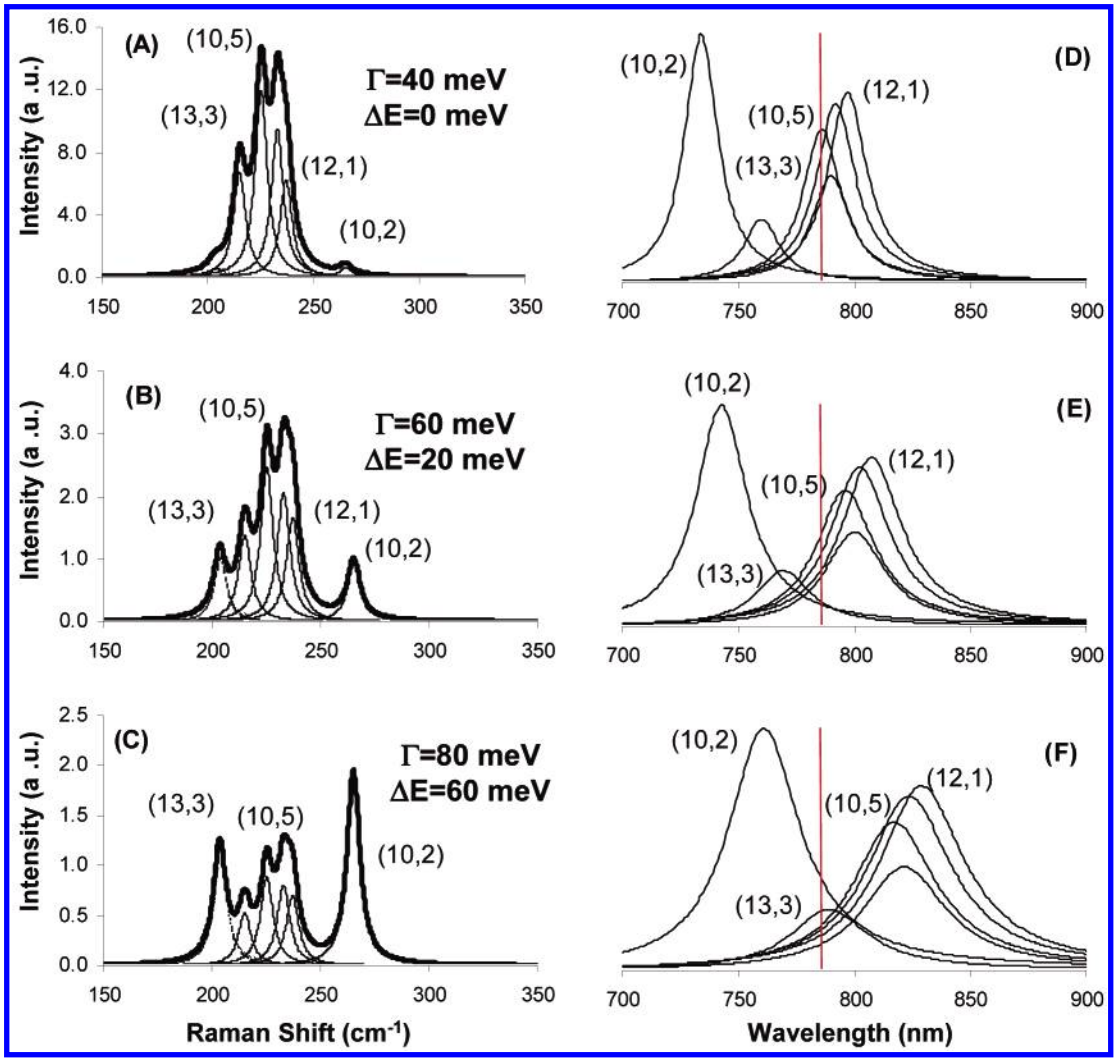


**Figure 3.** Simulated Raman spectrum at an excitation of 785 nm as a summation of Lorentzians with a deviation of 7 $cm^{-1}$ (from ref 2), using intensities calculated from two factors: the simplified excitation profile represented as eq 1 and the diameter-dependent concentration distribution in Figure 2. Spectra are parametric in relative energy shift $\Delta E$ and broadening $\Gamma$ (in eq 1): (a) $\Delta E = 0$, $\Gamma = 40$ meV; (b) $\Delta E = 20$, $\Gamma = 60$ meV; and (c) $\Delta E = 60$, $\Gamma = 80$ meV. Corresponding composite excitation profiles are shown in panels d, e, and f, respectively.

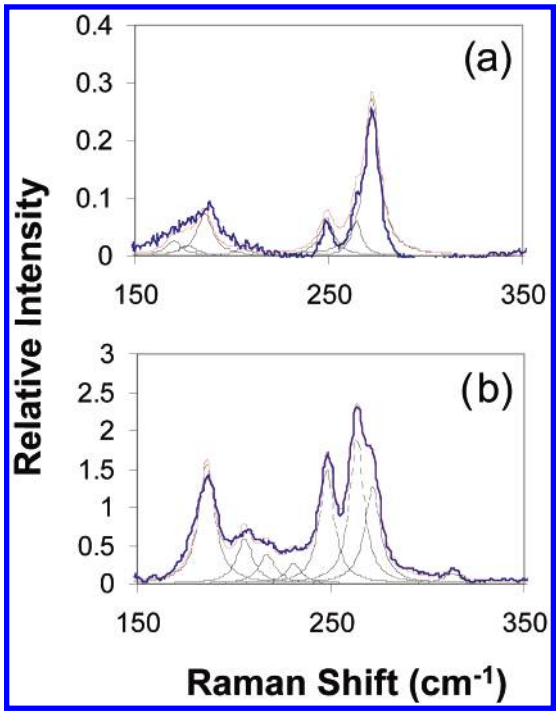


**Figure 4.** Raman spectra at an excitation of 514.5 nm for samples prepared with different morphological properties. RBM regions are shown for (a) a sample dispersed in aqueous solution using 1 wt % SDS at pH 10 and (b) the solid sample (HiPco SWNT) precipitated on a hot plate from SDS solution.

simplified as a delta function at energy $E_{(n,m)}$:[29]

$$I(E_{\text{Laser}}) \propto \frac{\frac{1}{\sigma\sqrt{4\pi}}\exp\left[-\frac{(d_t - d_{\text{mean}})^2}{4\sigma^2}\right]}{\left((E_{\text{Laser}} - E_{(n,m)} + \Delta E)^2 - \frac{\Gamma^2}{4}\right)\left((E_{\text{Laser}} - E_{\text{Phonon}} - E_{(n,m)} + \Delta E)^2 - \frac{\Gamma^2}{4}\right)}$$

Here, $E_{\text{Laser}}$ is the excitation energy with $\Delta E$ and $\Gamma$ is the energy shift on roping and peak broadening, based on the particular physical or chemical environment of the nanotubes. Figure 3a−c presents the simulated Raman spectrum with increasing $\Gamma$ and $\Delta E$. Despite the simplicity of the assumptions, the model qualitatively describes the spectral changes observed experimentally in Figure 1. An examination of the simulated excitation profiles, based on the aforementioned expression, provides some insight into the observed spectral changes (Figure 3d−f). The mode at 267 $cm^{-1}$ is the (10,2) nanotube that is initially off resonance in individually dispersed material. With aggregation, as transitions shift to lower energy, this feature is brought into resonance as others move away. Note that we have assumed, with no justification, that all transitions shift by the same amount, $\Delta E$. The magnitude of this constant shift is consistent with what is observed in the absorption spectrum[3] of roped material experimentally (~60 meV). The change in the line shape ($\Gamma$) is also well within that expected for nanotubes in bundles, as values as high as 120 meV have been reported for experimentally measured excitation profiles.[30]

Similar aggregation effects are noted at other Raman wavelengths. We include experimental data at 514.5 nm excitation, because this wavelength is frequently used to probe metallic nanotubes for HiPco samples. In this case, the v3 → c3 transitions of semiconducting nanotubes are initially off resonance (Figure 4a), whereas aggregation brings these features into resonance, as observed previously. As a result, the intensity of the feature at 190 $cm^{-1}$ attributed to semiconductors is sensitive to the aggregation state of the sample, as are high-frequency modes in this region (as shown in Figure 4b). In this case, however, several semiconducting modes seem to be convoluted, and the shift is merely a change in the excitation window. We cannot apply the same analysis, because no assignment for v3 → c3 yet exists.

Changes in the tangential-mode region of the Raman spectrum also complicate its utility in gauging changes in metallic and semiconductor concentration. As described previously, this mode splits into two components, because of differences in the force constants for the C−C vibration for bonds axial and circumferential to the tube. The latter is able to couple to the continuum of electronic transitions near the Fermi level for metallic nanotubes exclusively, and the result is a BWF line shape.[20] This line shape is frequently used to identify the presence of metallic nanotubes in the sample for this reason. However, it follows that this feature should also be sensitive to processes that affect the electronic continuum. This is, in fact, the case experimentally. It has been shown in previous work that this BWF feature can shift to higher wavenumbers and effectively become indistinguishable from the Lorentzian component with increasing $H^+$ concentration in solution.[22] Metallic nanotubes in bundles are known to undergo electronic perturbations, including the opening of a pseudo-gap, as documented earlier in both theoretical[27] and experimental work.[31] We underscore that aggregation and bundling of nanotubes causes changes to this BWF region; however, we include the spectral evidence for the samples discussed herein as Supporting Information for brevity.

## Conclusions

We have used Raman spectroscopy to probe the aggregation states of single-walled carbon nanotubes in solution and as solids. The orthogonal electronic dispersion that develops as a result of intertube electrical contact broadens and shifts the interband transitions to lower energy. We show that the magnitude of this shift is dependent on the extent of bundle organization and inter-nanotube contact area. Evidently, aggregation shifts the effective excitation profile and causes peaks to increase or decrease, depending on where the transition lies, relative to the excitation wavelength in the Raman spectrum. We model the result using a simplified $\delta$-function representation of nanotube electronic structure. The findings are particularly relevant for evaluating nanotube separation processes, where relative peak changes in the Raman spectrum can be confused for selective enrichment. This correlation should also assist in the development of highly dispersed composite materials.

**Acknowledgment.** This work was supported by the University of Illinois at Urbana/Champaign School of Chemical Sciences and the National Science Foundation (through Grant No. CTS-0330350). Funding from the Dupont Co. Molecular Electronics Group is also appreciated. C. Kittrell is acknowledged for useful discussions. The authors thank Y. Talmon for generating the cryo-TEM image in Figure 1.

**Supporting Information Available:** Raman spectroscopic characterization of two samples dispersed in SDS and two solid samples (HiPco SWNT and precipitate from an SDS solution). (PDF) This material is available free of charge via the Internet at http://pubs.acs.org.

## References and Notes


(1) Avouris, P. *Acc. Chem. Res.* **2002**, *35*, 1026.

(2) Bachilo, S. M.; Strano, M. S.; Kittrell, C.; Hauge, R. H.; Smalley, R. E.; Weisman, R. B. *Science* **2002**, *298*, 2361.

(3) O'Connell, M. J.; Bachilo, S. M.; Huffman, C. B.; Moore, V. C.; Strano, M. S.; Haroz, E. H.; Rialon, K. L.; Boul, P. J.; Noon, W. H.; Kittrell, C.; Ma, J. P.; Hauge, R. H.; Weisman, R. B.; Smalley, R. E. *Science* **2002**, *297*, 593.

(4) Roche, S. *Ann. Chim. (Paris)* **2000**, *25*, 529.

(5) Schmidt, G.; Malwitz, M. M. *Curr. Opin. Colloid Interface Sci.* **2003**, *8*, 103.

(6) Thostenson, E. T.; Ren, Z. F.; Chou, T. W. *Compos. Sci. Technol.* **2001**, *61*, 1899.

(7) Dresselhaus, M. S.; Dresselhaus, G.; Eklund, P. C. *Science of Fullerenes and Carbon Nanotubes*; Academic Press: San Diego, CA, 1996.

(8) Saito, R.; Dresselhaus, G.; Dresselhaus, M. S. *Physical Properties of Carbon Nanotubes*; Imperial College Press: London, 1998.

(9) Bronikowski, M. J.; Willis, P. A.; Colbert, D. T.; Smith, K. A.; Smalley, R. E. *J. Vac. Sci. Technol. A* **2001**, *19*, 1800.

(10) Thess, A.; Lee, R.; Nikolaev, P.; Dai, H. J.; Petit, P.; Robert, J.; Xu, C. H.; Lee, Y. H.; Kim, S. G.; Rinzler, A. G.; Colbert, D. T.; Scuseria, G. E.; Tomanek, D.; Fischer, J. E.; Smalley, R. E. *Science* **1996**, *273*, 483.

(11) Kuzmany, H.; Plank, W.; Hulman, M.; Kramberger, C.; Gruneis, A.; Pichler, T.; Peterlik, H.; Kataura, H.; Achiba, Y. *Eur. Phys. J. B* **2001**, *22*, 307.

(12) Zheng, M.; Jagota, A.; Semke, E. D.; Diner, B. A.; McClean, R. S.; Lustig, S. R.; Richardson, R. E.; Tassi, N. G. *Nature Mater.* **2003**, *2*, 338.

(13) Strano, M. S.; Dyke, C. A.; Usrey, M. L.; Barone, P. W.; Allen, M. J.; Shan, H. W.; Kittrell, C.; Hauge, R. H.; Tour, J. M.; Smalley, R. E. *Science* **2003**, *301*, 1519.

(14) Krupke, R.; Hennrich, F.; von Lohneysen, H.; Kappes, M. M. *Science* **2003**, *301*, 344.

(15) Chattopadhyay, D.; Galeska, I.; Papadimitrakopoulos, F. *J. Am. Chem. Soc.* **2003**, *125*, 3370.

(16) Chen, Z.; Du, X.; Du, M.-H.; Rancken, C. D.; Cheng, H.-P.; Rinzler, A. G. *Nano Lett.* **2003**, *3*, 1245.

(17) Sauvajol, J. L.; Anglaret, E.; Rols, S.; Alvarez, L. *Carbon* **2002**, *40*, 1697.

(18) Dresselhaus, M. S.; Dresselhaus, G.; Jorio, A.; Souza, A. G.; Saito, R. *Carbon* **2002**, *40*, 2043.

(19) Strano, M. S. *J. Am. Chem. Soc.* **2003**, *125*, 16148.

(20) Brown, S. D. M.; Jorio, A.; Corio, P.; Dresselhaus, M. S.; Dresselhaus, G.; Saito, R.; Kneipp, K. *Phys. Rev. B* **2001**, *63*.

(21) Stephan, C.; Nguyen, T. P.; de la Chapelle, M. L.; Lefrant, S.; Journet, C.; Bernier, P. *Synth. Met.* **2000**, *108*, 139.

(22) Strano, M. S.; Huffman, C. B.; Moore, V. C.; O'Connell, M. J.; Haroz, E. H.; Hubbard, J.; Miller, M.; Kittrell, C.; Sivarajan, R.; Hauge, R. H.; Smalley, R. E. *J. Phys. Chem. B* **2003**, *107*, 6979.

(23) Strano, M. S.; Moore, V. C.; Miller, M. K.; Allen, M. J.; Haroz, H. A.; Kittrell, C.; Hauge, R. H.; Smalley, R. E. *J. Nanosci. Nanotechnol.* **2003**, *3*, 81.

(24) Kavan, L.; Dunsch, L. *Nano Lett.* **2003**, *3*, 969.

(25) Valentini, L.; Cantalini, C.; Lozzi, L.; Armentano, I.; Kenny, J. M.; Santucci, S. *Mater. Sci. Eng. C* **2003**, *23*, 523.

(26) Moore, V. C.; Strano, M. S.; Haroz, E. H.; Hauge, R. H.; Smalley, R. E.; Schmidt, J.; Talmon, Y. *Nano Lett.* **2003**, *3*, 1379.

(27) Reich, S.; Thomsen, C.; Ordejon, P. *Phys. Rev. B* **2002**, *65*, 155411.

(28) Venkateswaran, U. D.; Rao, A. M.; Richter, E.; Menon, M.; Rinzler, A.; Smalley, R. E.; Eklund, P. C. *Phys. Rev. B* **1999**, *59*, 10928.

(29) Pimenta, M. A.; Marucci, A.; Empedocles, S. A.; Bawendi, M. G.; Hanlon, E. B.; Rao, A. M.; Eklund, P. C.; Smalley, R. E.; Dresselhaus, G.; Dresselhaus, M. S. *Phys. Rev. B* **1998**, *58*, 16016.

(30) Canonico, M.; Adams, G. B.; Poweleit, C.; Menendez, J.; Page, J. B.; Harris, G.; van der Meulen, H. P.; Calleja, J. M.; Rubio, J. *Phys. Rev. B* **2002**, *65*.

(31) Itkis, M. E.; Niyogi, S.; Meng, M. E.; Hamon, M. A.; Hu, H.; Haddon, R. C. *Nano Lett.* **2002**, *2*, 155.